https://doi.org/10.5194/egusphere-2026-5384
Preprint. Discussion started: 9 September 2026

Direct Measurements of N_2O_5 Reactivity in Salt Lake City Suggest the Aerosol Nitrate Effect Suppresses Additional $PM_{2.5}$ Accumulation

James A. Christie[1,†], Theo Severud[2], Logan Forshee[2], Vanessa Selimovic[2], Siyuan Wang[1], Shatabdi Roy[2], Holly P. Lawson[2], Maria A. Garcia[3], A. Gannet Hallar[3], Haley Humble[3], John C. Lin[3], Paquita Zuidema[1], Kerri A. Pratt[2,4], Cassandra J. Gaston[1,*]

[1]Department of Atmospheric Science, Rosenstiel School for Marine, Atmospheric, & Earth Sciences, University of Miami, Fl 33149, USA

[2]Department of Chemistry, University of Michigan, Ann Arbor, MI 48109, USA

[3]Department of Atmospheric Sciences, University of Utah, Salt Lake City, UT 84112, USA

[4]Department of Earth & Environmental Sciences, University of Michigan, Ann Abor, MI 48109, USA

[†]Present Affiliation: Geophysical Institute, University of Alaska, Fairbanks, AK 99775, USA

[*]Corresponding Author: Email: cgaston@miami.edu, Ph: (305) 421-4979

Abstract

Salt Lake City (SLC) frequently experiences severe wintertime pollution due to the accumulation of fine particulate matter, which is dominated by ammonium nitrate (AN) during atmospheric inversion events. Recent measurements in SLC have shown that heterogeneous reactions between gaseous dinitrogen pentoxide (N_2O_5) and ambient aerosol drives most AN accumulation in SLC. However, information is lacking on the ambient aerosol sources present, and how efficiently these particles react with N_2O_5 to form AN. As such, we deployed an ambient aerosol flow tube coupled to a chemical ionization mass spectrometer and particle sizing instrumentation at the University of Utah in winter to probe the reactive uptake of N_2O_5 (γN_2O_5) that leads to AN formation. Aerosol particle composition was measured from offline filter collections and ion chromatography to determine how different particle sources react with N_2O_5. Under inversion conditions, we measured suppressed values of γN_2O_5 (median $\gamma N_2O_5 = 0.03 \pm 0.04$) that decreased to as low as 0.001 when high AN was measured, suggesting that the nitrate effect suppresses γN_2O_5 by ~ 0.02 per night. Under clean conditions, we observed elevated values of γN_2O_5 (median $\gamma N_2O_5 = 0.06 \pm 0.05$) due to efficient heterogeneous reactions with mineral dust, ammonium sulfate, and road salt aerosol with no notable decrease in γN_2O_5 throughout clean periods. Using a 1-dimensional chemical box model, we find that aerosol nitrate accumulation is limited when γN_2O_5 is less than 0.01 throughout the evening. These results suggest that the most important influence on γN_2O_5 in wintertime SLC is the nitrate effect.

https://doi.org/10.5194/egusphere-2026-5384
Preprint. Discussion started: 9 September 2026

Short Summary:

To understand winter particulate pollution in Salt Lake City (SLC), we directly measured N_2O_5 reactive uptake and aerosol composition. We find reactions are efficient under clean conditions, but suppressed during polluted periods by particulate nitrate. A 1D model demonstrates that this suppressed uptake limits further particulate accumulation during persistent pollution episodes. These direct measurements and modeling results show the importance of N_2O_5 reactions in pollutant production in SLC.

1: Introduction

Wintertime pollution in Salt Lake City (SLC) exposes more than 2-million residents to concentrations of fine particulate matter less than 2.5µm ($PM_{2.5}$) that exceed national ambient air quality standards (NAAQS, 24-hr average $PM_{2.5} > 35 \mu g/m^3$) 11 to 18 times per year, with ambient $PM_{2.5}$ concentrations reaching 60 to 80 $\mu g/m^3$ (Baasandorj et al., 2017, 2018). The primary driver for these pollution events is persistent atmospheric inversions, which occur when cold air is trapped below a layer of warmer air, limiting vertical mixing and concentrating pollutants near the valley surface (Baasandorj et al., 2017; Ivey et al., 2019; Lareau et al., 2013). However, chemical pathways driving the accumulation of $PM_{2.5}$ under inversion conditions in SLC remain poorly constrained. Several field observations have identified ammonium nitrate (NH_4NO_3, referred to as AN hereafter) as the dominant component of $PM_{2.5}$ during inversion events (Franchin et al., 2018; Hansen et al., 2010; Kelly et al., 2013; Kuprov et al., 2014), with field and model-informed analyses suggesting that AN formation is limited by the production of nitric acid (HNO_3) (Baasandorj et al., 2017; Franchin et al., 2018; Kuprov et al., 2014; Mangelson et al., 1997; McDuffie et al., 2019). Recent results from the Utah Winter Fine Particulate Study (UWFPS) suggest that heterogeneous reactions between dinitrogen pentoxide (N_2O_5) and ambient aerosol aloft in the residual layer of an inversion account for 52 – 85% of the daily observed surface-level HNO_3 and AN production (McDuffie et al., 2019). To estimate HNO_3 production, McDuffie et al., (2019) modeled the reactivity of N_2O_5 with ambient aerosol, commonly referred to as the reactive uptake coefficient of N_2O_5 (γN_2O_5). While the results from McDuffie et al., (2019) provide critical insight on how N_2O_5 chemistry drives the production of secondary $PM_{2.5}$ in SLC, the box model used was unable to determine the cause of variability in γN_2O_5, limiting the ability of chemical models to predict $PM_{2.5}$ production in SLC.

The reaction mechanism leading to the formation of HNO_3 from N_2O_5, a nighttime product of the oxidation of nitric oxides ($NO + NO_2 \equiv NO_x$) with ozone (O_3) (shown in R1 – R2), occurs when N_2O_5 reacts with an aerosol (R3 – R4), also referred to as γN_2O_5 (Bertram & Thornton, 2009). Aqueous-N_2O_5 can then undergo a hydrolysis reaction to produce aqueous nitrate (R5) (Chang et al., 2011; Dentener & Crutzen, 1993; Morris & Niki, 1973; Mozurkewich & Calvert, 1988):

$$NO_{2(g)} + O_{3(g)} \rightarrow NO_{3(g)} \quad \text{(R1)}$$

https://doi.org/10.5194/egusphere-2026-5384
Preprint. Discussion started: 9 September 2026

$$NO_{3(g)} + NO_{2(g)} \leftrightarrow N_2O_{5(g)} \quad \text{(R2)}$$

$$N_2O_{5(g)} \leftrightarrow N_2O_{5(aq)} \quad \text{(R3)}$$

$$N_2O_{5(aq)} + H_2O_{(l)} \leftrightarrow NO^-_{3(aq)} + H_2ONO^+_{2(aq)} \quad \text{(R4)}$$

$$H_2ONO^+_{2(aq)} + H_2O_{(l)} \rightarrow H_3O^+_{(aq)} + HNO_{3(aq)} \quad \text{(R5)}$$

Reactions R4 + R5 will also yield a second HNO_3 molecule, with every molecule of N_2O_5 that reacts with water producing 2 molecules of HNO_3 (Chang et al., 2011). HNO_3 can then react with ammonia (NH_3), which partitions from the gas to the condensed phase, to form AN (R6) (Baasandorj et al., 2017; McDuffie et al., 2019):

$$HNO_{3(aq)} + NH_{3(aq)} \rightarrow NH_4NO_{3(aq)} \quad \text{(R6)}$$

The role of reactions R1 – R5 in the formation of HNO_3, and secondary $PM_{2.5}$, is thought to be limited by the availability of O_3 (Baasandorj et al., 2017), partially explaining observed maximum wintertime $PM_{2.5}$ concentrations of 60 to 80 μg/m^3 during multiday inversion events in SLC (Baasandorj et al., 2017; Lareau et al., 2013; Silcox et al., 2011; Whiteman et al., 2014). This is because under clean conditions in SLC, ozone is between 30 to 50 ppbv (Schnell et al., 2009), which rapidly depletes through the formation of HNO_3 via R1 – R3 under inversion conditions. This leads to O_3 titrating to non-detectable levels within 5 – 6 days (Baasandorj et al., 2017). However, no study to our knowledge has yet probed the role of changing particle composition caused by differing atmospheric conditions on the N_2O_5 reaction efficiency in SLC, which could also play a key, yet unexplored, role in secondary $PM_{2.5}$ accumulation.

Values of γN_2O_5 vary greatly depending on the chemical composition of the reacting aerosol (Ahern et al., 2018; Bertram & Thornton, 2009; Mitroo et al., 2019; Mozurkewich & Calvert, 1988; Roberts et al., 2009; Thornton & Abbatt, 2005). The presence of particulate nitrate (NO_3^-) and organics have been shown in the laboratory to suppress γN_2O_5 (Bertram & Thornton, 2009; Gaston, Thornton, et al., 2014; Mentel et al., 1999); for nitrate, this suppression is termed the 'nitrate effect' (Bertram & Thornton, 2009; Mentel et al., 1999). In contrast, increased concentrations of particulate chloride (Cl^-), sulfate (SO_4^{2-}), silicates commonly found in mineral dust, and aerosol liquid water enhance γN_2O_5 (Bertram & Thornton, 2009; Christie et al., 2025; Mitroo et al., 2019; Mozurkewich & Calvert, 1988; Royer et al., 2021; Staudt et al., 2019). However, these laboratory-derived trends do not fully capture observations of N_2O_5-aerosol interactions in field studies, in part due to the competing effects of complex particle composition on γN_2O_5 (Gaston, 2020; Li et al., 2025; McNamara et al., 2020; Mozurkewich & Calvert, 1988; Roberts et al., 2009; Shiraiwa et al., 2013), which is challenging to simulate under idealized laboratory conditions.

In this study, we directly measure γN_2O_5 on ambient aerosol for the first time in SLC, Utah during polluted and clean wintertime conditions. Bulk measurements of particle

https://doi.org/10.5194/egusphere-2026-5384
Preprint. Discussion started: 9 September 2026

composition were used to predict the effects of varying aerosol chemical composition under inversion and non-inversion conditions on values of γN_2O_5. We then probe the relationship between observed decreases in γN_2O_5 and $PM_{2.5}$ accumulation observed under inversion conditions in SLC using a 1-D chemical box model. The results presented herein show the effect of aerosol chemical composition on suppressing heterogeneous reactions, potentially limiting the accumulation of secondary $PM_{2.5}$.

2 – Methods

2.1: Site Description and On-Site Measurements

Direct measurements of γN_2O_5 and the collection of aerosol particles for offline analysis were conducted from January 27, 2024 through February 14, 2024 at the top of the William Browning Building (WBB) located on the University of Utah campus in Salt Lake City, Utah (40.456° N, 111.505° W, ~176 m above ground level). Ambient temperature (T), relative humidity (RH), ozone (O_3), $PM_{2.5}$ mass concentration, wind speed, and wind direction were measured on the WBB roof and obtained from the MesoWest WBB data repository (Horel et al., 2002). Co-located measurements by the Land-Atmosphere Interactions Research (LAIR) group used a Teledyne Model T200 Chemiluminescence Nitrogen Oxides Analyzer (Teledyne API, Inc.) to measure NO and total NO_x (NO + NO_2), which is then used to calculate NO_2, both of which were calibrated using a Model T750 Dilution Calibrator (Teledyne API, Inc.). Potential temperature profiles were obtained at the Salt Lake City International Airport (40.790°, -111.977°), located within the basin of the Salt Lake Valley, through the University of Wyoming's atmospheric sounding repository. Soundings were taken twice daily at 05:00 and 17:00 mountain standard time (MST). The potential temperature soundings (Figure S1) were used to calculate the valley heat deficit (VHD) as a means of determining if inversion conditions that favor pollution accumulation were reached (Whiteman et al., 2014). The VHD is discussed further in Section S1 of the supplementary information (SI).

Aerosol particles are routinely measured at the site. A custom-built aerosol inlet was used to pull air from 12.5 m above the roof of the WBB field site, with a total height of ~ 188 m above the basin floor, which is within the typical height of the nighttime residual layer for SLC (Lareau et al., 2013). Ambient air is pulled at a rate of 877.82 L/min through a 10.16 cm inner diameter (i.d). tube and travels 1.5 m to 0.64 cm stainless steel outer diameter (o.d.) sample pickoffs (Petersen et al., 2019). The sample pickoffs feed 1.7 to 2.7 L/min of air into 20.32 cm long, 0.65 cm o.d. copper tube that brings aerosol-laden air to the different aerosol measurement instruments including the custom-built ambient flow tube apparatus to measure γN_2O_5 (described in Section 2.2).

2.2 Direct Measurements of N_2O_5 Reactivity with Ambient Aerosols

γN_2O_5 was measured using a custom-built ambient flow tube (AFT) similar to the one described by Bertram et al., (2009). The AFT is comprised of a 15 cm i.d., 90 cm long, stainless

https://doi.org/10.5194/egusphere-2026-5384
Preprint. Discussion started: 9 September 2026

steel tube with conical stainless-steel end caps, which were coated with halocarbon wax (Halocarbon Corp.) to reduce wall reactions. Air was sampled from the WBB inlet through a filter manifold containing a 0.95 cm o.d. stainless steel 3-way actuated ball valve (Assured Automation; D33DAXV4B), which automatically switches between particle-free mode and aerosol sample mode every 30 minutes. When sampling ambient air, the air sample passes through a 90° turn that limits transmitted aerosol to $\leq$ 1 µm, then continues towards the AFT. When sampling particle-free air for background measurements, the air sample is filtered through a 5 µm pore size polytetrafluoroethylene (PTFE) filter (Whatman, PTFE Membrane Filter TE38), which decreased the aerosol reactive surface area concentration ([Sa]) by 95 to 99% throughout the study period. Either particle-free or ambient air then enter the AFT to react with N_2O_5 generated by the reaction of an excess of NO_2 (2 ppm standard; Airgas) with 700 ppb O_3 (2B Technologies, Inc.) to produce ~100 pptv N_2O_5 at a flow rate of 0.1 L/min. Additional information on the AFT and calibrations for γN_2O_5 is available in Section S2.1.

N_2O_5 was monitored at the exit of the AFT using an iodide (I^-) adduct quadrupole chemical ionization mass spectrometer (CIMS) from THS instruments (Liao et al., 2011; McNamara et al., 2019) and detected as $[I{\bullet}N_2O_5]^-$ at 235 amu. Further details on the CIMS are available in Section S2.2, including a tabulated list of the iodide adduct ions measured (Table S1**)**. Before and after the study period, we calibrated the AFT using commercially available sodium chloride (NaCl, Sigma-Aldrich $\geq$ 99% Purity), which was atomized to generate aerosol of a known reactivity with N_2O_5 (~0.03) and produce $ClNO_2$ with a yield of ~1 based on previous laboratory experiments (Behnke et al., 1997; Gaston & Thornton, 2016; Stewart et al., 2004; Thornton & Abbatt, 2005). Calibrations consistently showed the expected uptake kinetics and were independent of [Sa] shown in Figure S2. The method to convert the CIMS signal, which is normalized to $[I{\bullet}H_2O]^-$, to pptv for N_2O_5 is discussed in Section S2.3 and McNamara et al., (2019). Briefly, the CIMS was calibrated routinely (twice per hour) using a commercially available chlorine (Cl_2) permeation source, with the output verified offline daily (discussed in detail in Section 2.3). Using the Cl_2 calibration, we are then able to calculate the concentration of N_2O_5 using the relative sensitivity factor, for this instrument, previously determined by McNamara et al., (2019) of 0.85 for N_2O_5:Cl_2.

The particle number size distribution was measured from a second exit at the bottom of the AFT, through 1.02 m of 0.63 cm i.d. black conductive tubing, using a Scanning Mobility Particle Sizer (TSI Inc., 3787 CPC and TSI Inc., 3082 DMA) with a size range of 0.01 to 0.7 µm. During the first sampling period of the field study (January 27, 2024, to February 5, 2024), an Optical Particle Sizer (TSI Inc., 3330 OPS) with a size range of 0.07 to 20 µm was also used to extend the aerosol particle size distribution measurement to larger sizes. However, approximately 94% of the aerosol number concentration was in the 0.02 to 0.2 µm size range during the study, as shown in Figure S3. To increase the aerosol residence time in the flow apparatus, the OPS was removed during the second sampling period of the field study (February 7, 2024, to February 14, 2024). A flow diagram for the apparatus and sampling setup is shown in Figure S4**.**

https://doi.org/10.5194/egusphere-2026-5384
Preprint. Discussion started: 9 September 2026

By measuring N_2O_5 and the particle number size distribution, which is converted to the total available surface area for the reactive uptake of N_2O_5, at the exit of the AFT, γN_2O_5 can be quantified using the particle modulation technique (Bertram et al., 2009). We ensured N_2O_5 wall loss was consistent within the AFT between the ambient and filtering state by injecting particle-free air upstream of the AFT and shifting the 3-way valve between ambient and background, which showed no change in N_2O_5 signal. Since N_2O_5 wall loss is negligible between the ambient and filtered states, we can calculate the pseudo first order rate constant between N_2O_5 and the ambient particle population (k_{het}) every hour using Equation 1:

$$k_{het} = -\frac{1}{t_{res}} \times \ln \frac{N_2O_{5(amb)}}{N_2O_{5(bkg)}} \quad (1)$$

where t_{res} is the residence time of the flow tube in seconds (360 seconds during the first sampling period with the OPS, and 565 seconds during the second sampling period without the OPS), $N_2O_{5(amb)}$ represents the average normalized N_2O_5 signal when ambient aerosol is present, and $N_2O_{5(bkg)}$ represents the average normalized N_2O_5 signal when the sampled air passes through the filter. The observed k_{het} was then used to calculate γN_2O_5, with the inclusion of gas-phase diffusion limitations (Fuchs & Sutugin, 1971) using Equation 2:

$$\frac{1}{\gamma_{N_2O_5}} = \frac{\omega[Sa]}{4k_{het}} - \frac{0.75+0.283\overline{K_n}}{\overline{K_n}+(1+\overline{K_n})} \quad (2)$$

where [Sa] is the aerosol reactive surface area concentration in cm^2/cm^3, ω is the mean molecular speed of N_2O_5 in cm/s (approximately 2.4×10^4 throughout the study), and $\overline{K_n}$ is the dimensionless Knudsen number calculated in Section S2.4.

Several factors outside of particle composition can affect the measured value of γN_2O_5 including changes in temperature and relative humidity affecting the wall loss of N_2O_5 to the reactor (Bertram et al., 2009; Riedel et al., 2012). We removed any uptake coefficients where ambient RH and T varied by more than 2% and 2°C, respectively, during the hour-long sampling period. Fluctuations in NO have previously been shown to affect the NO_3/N_2O_5 equilibrium within the AFT, which can lead to artificially high uptake coefficients (Bertram & Thornton, 2009; Riedel et al., 2012). Previous experiments using the AFT, such as those reported by Riedel et al., (2012) and Bertram et al., (2009), suggest any uptake coefficient observed when NO is greater than 1 ppbv should be removed. However, ambient concentrations of NO frequently exceeded 1 ppbv throughout the study due to the field site being located near a busy road. Due to the elevated NO observations during our study, we instead remove any values of γN_2O_5 where both the variability of NO is greater than 1 ppbv (where variability is quantified as 1σ in NO concentration over the entire 1-hr sampling cycle) and when 'spikes' are present in the normalized N_2O_5 signal after steady-state conditions are established. Since elevated concentrations of NO were observed throughout, we are likely measuring the upper limit of γN_2O_5 (Bertram et al., 2009). The lower limit of [Sa] where we can confidently detect γN_2O_5 with the AFT was calculated from the variation of N_2O_5 wall loss rates (Gaston et al., 2014) and

https://doi.org/10.5194/egusphere-2026-5384
Preprint. Discussion started: 9 September 2026

was estimated to be ~ 50 $\mu m^2/cm^3$. Any values of γN_2O_5 calculated when [Sa] was below 50 $\mu m^2/cm^3$ were filtered out.

2.3: Particle Collection and Chemical Composition Analysis

Size-resolved particles were collected daily over 23-hour periods from approximately 18:00 to 17:00 MST using a micro-orifice uniform deposit impactor (MOUDI, Model 110-NR, MSP Corp.). The MOUDI sampled through 43 cm of 0.95 cm i.d. copper tubing before a 0.95 o.d. quarter-turn valve upstream of the MOUDI and operated at a flow rate of approximately 30 L/min for the duration of the study. Samples were collected on 5 µm pore size PTFE filters (Whatman, PTFE Membrane Filter TE38) and preserved in petri dishes. The filters were then frozen until offline analysis to reduce sample re-volatilization. Detailed information on the filter extraction and sample preparation for offline analysis is described in Section S3.1. We focus on the analysis of particles from stage 8 (0.18 – 0.32 µm), stage 7 (0.32 – 0.56 µm), stage 6 (0.56 – 1.0 µm) and stage 5 (1.0 – 1.8 µm) based on the size distributions of particles exiting the flow tube.

Two ion chromatography (IC) instruments (Thermo Fisher Scientific) were used for measurements of cations (Dionex Aquion; Li^+, Na^+, NH_4^+, K^+, Mg^{2+}, Ca^{2+}) and anions (Dionex ICS-2100; NO_2^-, NO_3^-, Cl^-, Br^-, SO_4^{2-}, PO_4^{3-}), with detection limits for cations and anions shown in Table S2. Water-soluble ions were extracted from the filters using the same method previously described by Gaston et al., (2017). Briefly, the filters were soaked in 30 mL of ultrapure Milli-Q water (>18 MΩ resistivity), then sonicated at 60 ºC for 75-minutes and then cooled to room temperature (~ 25 ºC) for 3 hours. The suspension was then filtered using a 0.22 µm syringe filter (CELLTREAT Scientific Products) before being manually injected into both IC systems. All sample analyses were performed in triplicate. Further details on the IC system configuration are available in Section S3.1. Raw chromatographic data were then imported into the TAG ExploreR iNtegration package (TERN; Aerodyne Research Inc.), which uses an Igor Pro peak fitting software package (WaveMetrics, Igor Pro 8.04) to fit chromatographic peaks (Isaacman-VanWertz et al., 2017). The methods for calculation of concentrations are available in Section S3.2.

Thermodynamic modeling was used to predict the aerosol chemical composition throughout the field study using the soluble ion concentrations measured using IC. We utilized ISORROPIA-II (Fountoukis & Nenes, 2007), which was run for each study day at the 24-hour averaged temperature and RH values. The model was run under stable conditions to allow aerosol to precipitate under supersaturated conditions.

2.4: 1-D Chemical Box Model

We extend our field measurements to estimate the impact of inversion conditions on values of γN_2O_5 and (ammonium) nitrate production in the residual layer of the SLV using a one-dimensional (1-D) chemical model (Jeong et al., (2023), McNamara et al., (2020), and Wang et

https://doi.org/10.5194/egusphere-2026-5384
Preprint. Discussion started: 9 September 2026

al., (2020)). Briefly, the 1-D model simulates prognostic equations, turbulent transport, gas-phase chemistry, phase-transfer, aqueous phase chemistry, and heterogeneous chemistry, which are discussed in Section S4. The model consists of 50 linearly spaced vertical layers that are 20 m in height providing simulations up to 1000 m above surface level. The formulas describing turbulent transport and its parameterization are discussed by Wang et al., (2020) and discussed in Section S4.1. Gas-phase chemical reactions are simulated using the same method described by Wang and Pratt, (2017), with additional gas-phase chemical reactions involving $C_1 - C_4$ hydrocarbons (methane, ethane, propane, i-/n-butane) and oxidation products from the Master Chemical Mechanism (MCM, version 3.3.1) (Jenkin et al., 2003; Saunders et al., 2003), which is described in Section S4.2. Heterogeneous reactions are predicted in the model, with the equation discussed in Section S4.2. We used the Bertram and Thornton parameterization (herein referred to as BT09, (Bertram & Thornton, 2009)) to predict values of γN_2O_5 within the model, with the equation for the parameterization shown in Section S4.3. Values of aerosol chloride, aerosol nitrate, and aerosol liquid water content are predicted within the model. We note that aerosol liquid water was overpredicted relative to the E-AIM model (Wexler & Clegg, 2002), thus we applied a correction factor to improve agreement between the two models, which is discussed in Section S4.3 and shown in Figure S5.

The model predicts the emissions of NO_x, NH_3, SO_2, and other gaseous species at the surface using the Greenhouse Gas and Air Pollutants Emissions Systems (GRA^2PES) emissions inventory (Lyu et al., 2025) after assuming initial mixing ratios of gas and aerosol informed by previous ambient observations (Baasandorj et al., 2017, 2018) as well as observations from this study (see Table S3 for initial mixing ratios). Meteorological conditions for the inversion period (e.g., RH, temperature, wind speed, wind direction, inversion height) were informed by soundings from Salt Lake City International Airport discussed in Section 2.1. The inversion observed on February 7, 2016, was used for this model, which presented a daytime planetary boundary layer height of 600 m and nighttime planetary boundary layer height of 350 m. The residual layer within the model is simulated between the daytime and nighttime boundary layer altitudes, with a depth of ~ 250 m between 350 and 600 m above ground level, which was simulated using inversion observations in SLC (Sun & Holmes, 2019). The simulation was run for a total of 104-hours, with the first 17 hours removed from the analysis to allow the model to properly mix surface emissions into the residual layer.

Section 3: Results and Discussion

3.1: Temporal Variability in Aerosol Soluble Ion Content and γN_2O_5 Under Inversion and Non-Inversion Conditions

Figure 1 provides an overview of clean and polluted periods observed throughout the study. The valley heat deficit (VHD, Figure 1A), hourly averaged concentrations of NO_x (Figure 1B), 24-hour averaged $PM_{2.5}$ concentration and soluble inorganic ion concentration (Figure 1C), and values of γN_2O_5 (Figure 1D) are shown from January 27, 2024 to February 14, 2024.

https://doi.org/10.5194/egusphere-2026-5384
Preprint. Discussion started: 9 September 2026

Tabulated 24-hr median values of γN_2O_5 and daily 0.18 – 1.8 µm PM soluble ion concentrations are also available in Tables S3 and S4, respectively. We identified four different atmospheric stability periods throughout the campaign: Two periods of atmospheric stability, when mild inversions occurred allowing pollutants to build up, were observed from January 27 to January 31 (stable period 1) and February 11 to February 14 (stable period 2); two periods of clean air were observed from February 1 to February 5 (clean period 1) and February 7 to February 10 (clean period 2).

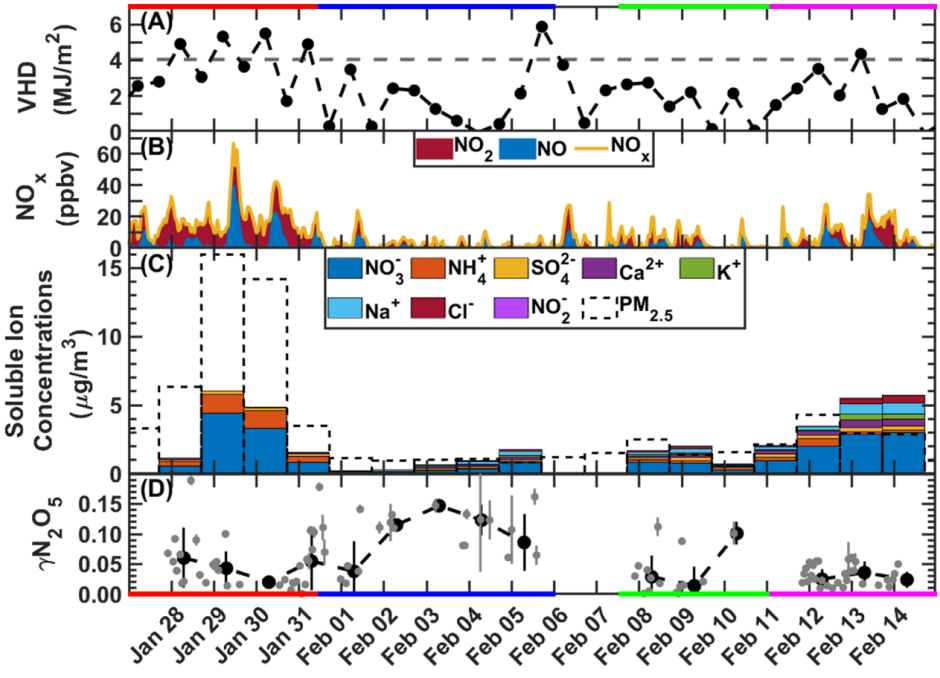

Figure 1: Times series of (A) VHD, (B) hourly NO_x concentrations, (C) daily $PM_{0.18\text{-}1.8}$ soluble ion and total $PM_{2.5}$ mass concentrations, and (D) measured values of γN_2O_5 from January 27 to February 15, 2024. Colored lines on the x-axis denote stable period 1 (red), clean period 1 (blue), clean period 2 (green), and stable period 2 (magenta). The grey markers for γN_2O_5 represent individual measured values of γN_2O_5 with error bars denoting their 95% confidence interval. The black markers for γN_2O_5 represent the 24-hr median with the error bars representing standard deviation of the individual values collected over the 24-hour period. We note that a snow event occurred during clean period 2.

3.1.1: Stable Period 1

Stable period 1 (January 27 to January 31) was classified as an inversion period by the VHD exceeding the 4.04 MJ/m^2 critical threshold (Baasandorj et al., 2017; Whiteman et al., 2014) during the 05:00 MST (evening) soundings (Figure 1A). We note that the VHD during the 17:00 MST (daytime) soundings were below the critical threshold, though the potential

https://doi.org/10.5194/egusphere-2026-5384
Preprint. Discussion started: 9 September 2026

temperature soundings in Figure S1 show weak daytime inversions. Other indicators of an inversion during stable period 1 were elevated concentrations of NO_x (Figure 1B) and $PM_{2.5}$ (24-hr average in Figure 1C, hourly average in Figure S6), with observed 4-day averages of 21 ppbv and 12 $\mu g/m^3$, respectively. Inversion periods can also be identified by the depletion of O_3, caused by the formation of NO_2, N_2O_5, and HNO_3 in the residual layer (Baasandorj et al., 2017). Stable period 1 showed reduced concentrations of O_3 (4-day average of 18 ppbv) relative to clean conditions (~ 30 ppbv), further supporting the presence of an inversion (Baasandorj et al., 2017, 2018; Whiteman et al., 2014).

The largest contributions of particulate nitrate (NO_3^-) and ammonium (NH_4^+) were measured during stable period 1, representing 61 ± 11 and 27 ± 4% of the total $PM_{0.18\text{-}1.8}$ measured by IC (Figure S7). Both SO_4^{2-} and Ca^{2+} contributed to the total measured $PM_{0.18\text{-}1.8}$ mass (7.2 ± 0.1 and 3.2 ± 0.1%, respectively). We used the ISORROPIA-II model to understand the likely aerosol chemical composition under ambient conditions (Fountoukis & Nenes, 2007), with the IC inputs shown in Table S5. The model output suggests the principal compound present during stable period 1 is AN representing 90 ± 15% of the measured $PM_{0.18\text{-}1.8}$. Elevated concentrations of AN is expected during inversion periods in the SLV (Baasandorj et al., 2017, 2018; Kuprov et al., 2014; McDuffie et al., 2019). We do note that aerosol liquid water is included in this mass percentage estimate as we assume the AN is hydrated during typical ambient conditions. Gypsum ($CaSO_4$) has previously been shown to be a marker for mineral dust from the Great Salt Lake (Christie et al., 2025), which is the other principal chemical during stable period 1, as indicated by a 4-day average $CaSO_4$ mass percentage of 7 ± 7%. SO_4^{2-} may also be present as ammonium sulfate ($(NH_4)_2SO_4$), which is common in the SLV (Franchin et al., 2018), though our ISORROPIA estimates did not predict $(NH_4)_2SO_4$ to be present.

The average value of γN_2O_5 over the 4-day period was 0.04 ± 0.02 (average ± standard deviation) and ranged from 0.001 ± 0.001 to 0.189 ± 0.008 (individual γN_2O_5 ± 95% confidence interval). The first day of the inversion (January 27 to 28) showed the highest values of γN_2O_5, with a 24-hr median of 0.06 ± 0.05, as well as higher relative mineral dust content and some hydrated AN (13% and 83%, respectively). The third day of the inversion (January 29 to 30) showed the lowest value of γN_2O_5 (24-hr median = 0.020 ± 0.006) and highest predicted mass percentage of hydrated AN (96%) as well as lower gypsum (2%), indicating a low abundance of soluble minerals from dust. We attribute the reduction in measured γN_2O_5 with elevated AN to the aerosol nitrate effect, which inhibits the heterogeneous hydrolysis reaction with N_2O_5 (Mentel et al., 1999) and agrees with prior wintertime observations that estimated γN_2O_5 in Colorado (Wagner et al., 2013). Our observations during this stable period also suggest that as AN accumulates, values of γN_2O_5 decrease by ~ 0.02 per night during the early stages of a persistent inversion, potentially limiting the rate of AN production as γN_2O_5 decreases due to the aerosol nitrate effect.

3.1.2: Clean Period 1

https://doi.org/10.5194/egusphere-2026-5384
Preprint. Discussion started: 9 September 2026

Clean period 1 (February 1 to February 5) was the least polluted period during the campaign as indicated by a VHD below the critical threshold suggesting an inversion did not occur, low NO_x (5-day average = 3 ppbv) and $PM_{2.5}$ (5-day average = 1 µg/m^3) concentrations, and background O_3 concentrations (5-day average = 33 ppbv). Relative to stable period 1, elevated $PM_{0.18\text{-}1.8}$ mass fractions of Na^+, Ca^{2+}, K^+, SO_4^{2-}, and Cl^- (20 ± 10, 15 ± 5, 2 ± 3, 18 ± 9, and 5 ± 5%, respectively) and reduced mass fractions of NH_4^+ and NO_3^- (18 ± 12 and 22 ± 21%, respectively) were observed. ISORROPIA-II predicted that the principal aerosol type present during clean period 1 was mineral dust, indicated by elevated relative abundances of $CaSO_4$ (30 ± 39%), Na^+ (11 ± 9%), and Cl^- (2 ± 3%). We suspect ISORROPIA-II is overpredicting $CaSO_4$ and underpredicting ammonium sulfate ($(NH_4)_2SO_4$), as $(NH_4)_2SO_4$ is expected to be ~ 13% of the aerosol mass under wintertime clean conditions (Franchin et al., 2018), though ISORROPIA predicted no $(NH_4)_2SO_4$. During clean period 1, the predicted AN was lower than during stable period 1, with notable reductions in total predicted mass percentages of solid-NH_4NO_3 (0%), aqueous NH_4^+ (7.4%) and NO_3^- (12.8%). KCl is also predicted by ISORROPIA and has an average mass percentage of 2 ± 3% during clean period 1, likely indicating the presence of residential wood burning (Kelly et al., 2013).

The highest values of γN_2O_5 measured during the campaign were during clean period 1. The 5-day average value of γN_2O_5 was 0.10 ± 0.04 and ranged from 0.018 ± 0.001 to 0.16 ± 0.01. Observed values of γN_2O_5 were highest on February 3rd, with a 24-hr median of 0.15 ± 0.01. Previous studies have observed comparable values of γN_2O_5 for mineral dust under idealized laboratory conditions with high values of γN_2O_5 explained by the high reactivity of N_2O_5 with silicates (Christie et al., 2025; Mitroo et al., 2019; Royer et al., 2021; Tang et al., 2012, 2014). The combination of similar values of γN_2O_5 to laboratory observations and elevated $CaSO_4$ suggest that mineral dust is likely driving the high values of γN_2O_5 under clean conditions. Other suspected aerosol sources that may be contributing to elevated values of γN_2O_5 include $(NH_4)_2SO_4$, which typically has a N_2O_5 reactivity coefficient of 0.03 depending on RH (Gaston & Thornton, 2016; Hu & Abbatt, 1997; Kane et al., 2001). We note that the low concentration of $PM_{2.5}$ during clean period 1 led to a majority of ambient γN_2O_5 observations (~ 85%) being removed as the observed [Sa] (see Figure S6 and Table S4 for [Sa] observations) was below the detectable [Sa] limit of the AFT. Thus, we are only reporting values of γN_2O_5 during periods when concentrations of ambient $PM_{2.5}$ were high enough for the AFT to be operable. We also note that most measurements during clean period 1 occurred near the detectable limit of the AFT, which may result in values of γN_2O_5 that are biased high suggesting that the γN_2O_5 are upper limits.

3.1.3: Clean Period 2

Clean period 2 (February 7 to 10) had average concentrations of $PM_{2.5}$, NO_x, and O_3 similar to clean period 1 (2 µg/m^3, 4 ppbv, and 31 ppbv, respectively). Mass percentages of NO_3^- (43 ± 7%) were slightly elevated relative to clean period 1, likely due to the elevated VHD on February 7th through 9th, though similar mass percentages of Na^+, NH_4^+, K^+, Ca^{2+}, SO_4^{2-}, and Cl^-

https://doi.org/10.5194/egusphere-2026-5384
Preprint. Discussion started: 9 September 2026

(11 ± 2, 13 ± 7, 6 ± 2, 9 ± 3, 12 ± 2, and 6 ± 4%, respectively) were observed. High NO_3^- and low NH_4^+ mass concentrations suggest that AN is not the most abundant aerosol type during clean period 2 and may instead indicate aged mineral dust and/or road salt, which have previously been shown to act as a sink to N_2O_5 and HNO_3 (Hrdina et al., 2021; McNamara et al., 2020). ISORROPIA-II does suggest minor contributions of AN to the aerosol population (indicated by solid-NH_4NO_3 mass percentage of 3 ± 5, respectively). We partially attribute the enhanced AN observations, compared to clean period 1, to the occurrence of a snow event with cold temperatures and high humidity that can favor AN accumulation even when no inversion is present (Franchin et al., 2018). Other aerosol sources predicted by ISORROPIA-II include mineral dust (indicated by $CaSO_4$ = 10 ± 5%) and sodium nitrate ($NaNO_3$) representing aged road salts (McNamara et al., 2020), and aqueous Na^+ and Cl^- indicating deliquesced fresh road salts (Kolesar et al., 2018; McNamara et al., 2020).

Values of γN_2O_5 during clean period 2 ranged from 0.001 ± 0.001 to 0.112 ± 0.016 and were notably lower than clean period 1. The reduction in γN_2O_5 can likely be attributed to a mild nitrate effect, indicated by the enhanced concentrations of $NaNO_3$ (likely indicative of aged road salt), AN, and aqueous NO_3^- during this period. We also observed that road salts were applied during clean period 2. The presence of road salts during clean period 2 is supported by recent laboratory measurements, which show similar values of γN_2O_5 (γN_2O_5 = 0.003 to 0.067) (Christie et al., 2026) to the ambient values of γN_2O_5 observed during clean period 2. The enhanced NO_3^-, Na^+, Cl^-, and $NaNO_3$ relative to clean period 1 suggests that increases in the contribution of road salt aerosol to the aerosol population, reductions in highly reactive mineral dust concentrations, and the nitrate effect are responsible for the reduction in γN_2O_5 during clean period 2, relative to clean period 1.

3.1.4: Stable Period 2

A second mild inversion period was observed during stable period 2 (February 11 to February 14), which occurred after the snow event observed during clean period 2. During this inversion period, NO_3^- remained the dominant species, with an average mass percentage of 54 ± 4%. However, the mass percentage of NH_4^- (7 ± 7%) was reduced relative to the first polluted period, suggesting that AN was not dominant. Instead, ISORROPIA-II simulations suggest the presence of $NaNO_3$, $CaSO_4$, and $Ca(NO_3)_2$, which indicate aged road salts and aged mineral dust (Hrdina et al., 2021; McNamara et al., 2020). During this time frame, the average value of γN_2O_5 was 0.03 ± 0.01 and ranged from 0.010 ± 0.001 to 0.061 ± 0.004, which matches previous measurements of γN_2O_5 for mineral dust and road salts from SLC (Christie et al., 2025, 2026). The lower values of γN_2O_5 relative to clean period 2, as well as the suspected presence of aged mineral dust indicated by $Ca(NO_3)_2$, suggests that the nitrate effect is driving further reductions in observed γN_2O_5 between clean period 2 and stable period 2.

3.1.5: Influence of Bulk Aerosol Chemical Composition on γN_2O_5

https://doi.org/10.5194/egusphere-2026-5384
Preprint. Discussion started: 9 September 2026

To examine the impact of changing aerosol chemical composition on observed values of γN_2O_5, we show the relationship between 24-hr median values of γN_2O_5 and daily bulk soluble ion concentrations in Figure S8. In this analysis, we do not include K^+ due to limited observations during the sampling period or data from 02/01 and 02/02 due to NO_3^- being uncharacteristically low for SLC. Negligible correlations ($R^2 < 0.2$) between γN_2O_5 and Na^+, NH_4^+, and Cl^- were observed, likely due to several sources of ions which present varying reaction rates with N_2O_5. Moderate correlations ($R^2 > 0.4$) were observed between γN_2O_5 and SO_4^{2-}, NO_3^-, and Ca^{2+}. Molar abundance of Ca^{2+} and SO_4^{2-} exhibit positive correlations with γN_2O_5 (R^2 both equal 0.4), likely due to the influence of mineral dust and ammonium sulfate enhancing N_2O_5 reactivity. NO_3^- shows a negative correlation with γN_2O_5 ($R^2 = 0.5$), which we attribute to the aerosol nitrate effect.

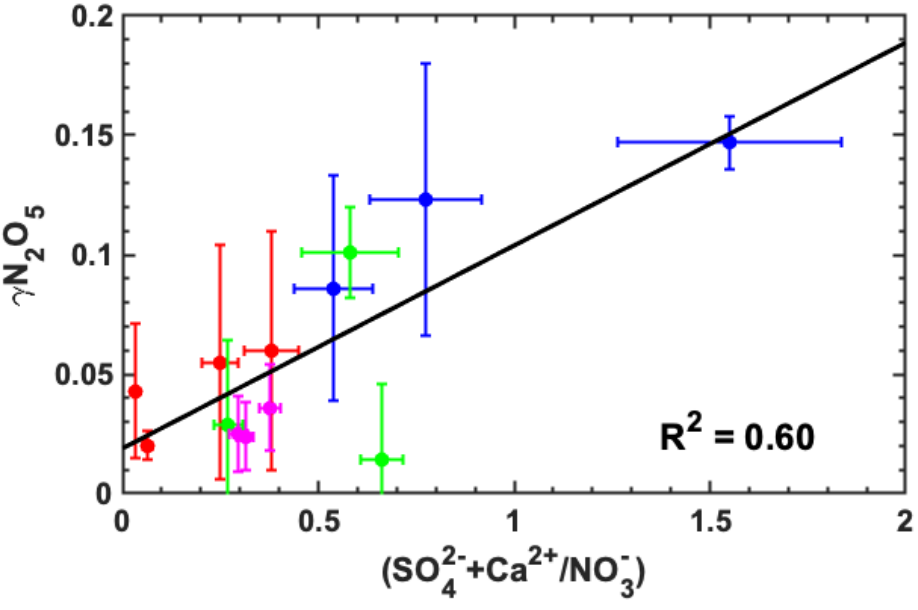

Figure 2: Correlation between the relative mole abundance of 'reactive' (SO_4^{2-} and Ca^{2+}) and 'unreactive' (NO_3^-) ions and 24-hr median values γN_2O_5. Colors denote stable period 1 (red), clean period 1 (blue), clean period 2 (green), and stable period 2 (magenta). Error bars represent the 95% confidence interval of γN_2O_5 during the sampling period and error bars for the relative mole abundances represent the 95% confidence interval for individual daily soluble ion measurements.

To better represent the influence of the relative abundances of reactive (Ca^{2+} and SO_4^{2-}) and unreactive (NO_3^-) ions on aerosol reactivity with N_2O_5, we calculate the ratio of reactive to unreactive compounds and their relationship with γN_2O_5 in Figure 2. The relative ratio of reactive/unreactive compounds shows a strong positive correlation ($R^2 = 0.6$) with N_2O_5. This strong correlation suggests that under clean conditions, the increased abundance of mineral dust

https://doi.org/10.5194/egusphere-2026-5384
Preprint. Discussion started: 9 September 2026

and ammonium sulfate likely drives the high observed values of γN_2O_5, while NO_3^- (either from AN or aged road salts and aged dust) is responsible for the low observed values of γN_2O_5 under polluted conditions. If the reactive uptake of N_2O_5 is indeed the key driver of nitrate accumulation and wintertime PM, then Figure 2 also demonstrates that the aerosol nitrate effect may play a pivotal role in suppressing further fine PM accumulation during prolonged inversion periods (Wagner et al., 2013). We further explore this possible control on AN accumulation with a 1-D model in the next section.

Section 3.2: Modeled Sensitivity of $PM_{2.5}$ Accumulation to Values of γN_2O_5

A 1-D chemical model was used to determine if the suppression of N_2O_5 reactivity due to the aerosol nitrate effect can inhibit the accumulation of secondary-PM during an inversion event. During the first night of the simulation (hours 17 to 32), average values of γN_2O_5 within the nighttime residual layer decrease from 0.029 to 0.005, and particulate nitrate increased by 9 $\mu g/m^3$ as shown in Figure 3. The model's simulations are consistent with observations of nighttime nitrate production by McDuffie et al., (2019) of 6 to 10 $\mu g/m^3$ per night. During the second evening (hours 41 to 56), values of γN_2O_5 ranged from 0.016 to 0.001. The higher predicted γN_2O_5 at the beginning of the evening is likely due to minor depositional losses of nitrate (indicated by a nighttime decrease in nitrate), slower nitrate production during the daytime, and regeneration of Cl^- from emissions and HCl uptake shown in Figure S9. The production of nitrate on the second night remained high at 8 $\mu g/m^3$ despite a 72% decrease in values of γN_2O_5. On the third night (hours 65 to 80), N_2O_5 reactivity ranged from 0.008 to 0.001, and the total nighttime production of nitrate was lower at 4 $\mu g/m^3$, which we attribute to the reduced γN_2O_5 values. On the fourth night (hours 89 to 104), γN_2O_5 remained low ranging from 0.007 to 0.001, and the total nitrate production was only 1 $\mu g/m^3$. The reduction in total nighttime nitrate accumulation between night 1 (9 $\mu g/m^3$) and night 4 (1 $\mu g/m^3$) suggests that as values of γN_2O_5 decrease in the nighttime residual layer, total nighttime nitrate production slows down. The cumulative 'end of night' nitrate mass concentration also levels out to ~25 $\mu g/m^3$, as shown by the logarithmic increase in nitrate between night 1 and night 4 of the simulation. The consistent mass concentration of nitrate after the third night, despite low values of γN_2O_5, can likely be attributed to the increase in aerosol reactive surface area [Sa] (see Figure S10) potentially driving the end of night cumulative aerosol nitrate mass concentration of ~25 $\mu g/m^3$ predicted during the third and fourth night of the simulation.

Since this model utilizes the BT09 parameterization (Bertram & Thornton, 2009), we are likely underpredicting values of γN_2O_5 during the first night of the simulation. This is because the BT09 parameterization only includes the competing effects of NO_3^-, Cl^-, and aerosol liquid

https://doi.org/10.5194/egusphere-2026-5384
Preprint. Discussion started: 9 September 2026

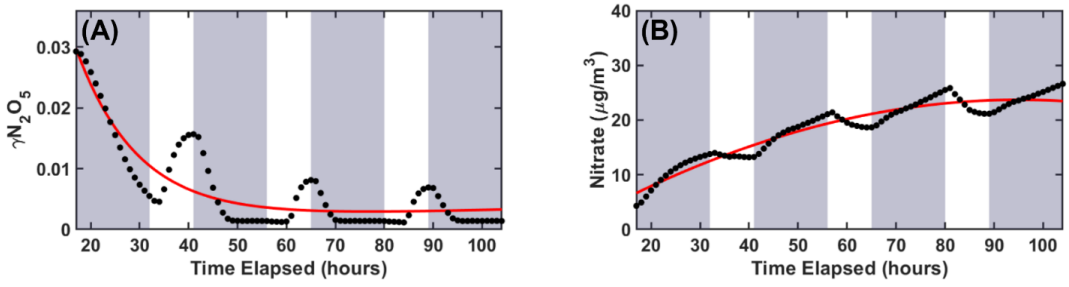

Figure 3: Timeseries (4-night) of values of γN_2O_5 (A) and nitrate concentration (B) as a function of model simulation time in the residual layer (height of 350 – 600 m A.G.L). The red line represents the (A) exponential decay in nighttime values of γN_2O_5 and (B) the polynomial fit in nighttime nitrate concentrations. The dark blue shaded regions represent nighttime periods in the simulation, where the solar zenith angle was < 85°. Unshaded regions are not included in the best fit lines.

water on values of γN_2O_5. Previous studies have shown that BT09 typically underpredicts values of γN_2O_5 in dust-rich regions such as the Salt Lake Valley (Christie et al., 2025; Mitroo et al., 2019; Tang et al., 2012, 2014). Observations by McDuffie et al., (2019) and this study, suggest values of γN_2O_5 can exceed 0.1 in the SLV, which is beyond the upper limit of what the BT09 parameterization can predict. To better understand the impact of high values of N_2O_5-aerosol reactivity on nitrate production, we subsequently ran a sensitivity check where values of γN_2O_5 were constant at 0.1, 0.08, 0.06, 0.04, 0.02, 0.015, 0.01, 0.0075, 0.005, 0.0025, 0.001, 0.0005, and 0.0001 to represent the full range of γN_2O_5 observed. We do not include daytime HNO_3 formation via the OH oxidation mechanism in these simulations. A comparison between model runs with and without daytime nitrate production, shown in Figure S11, suggests that removing the daytime OH oxidation mechanism decreases nitrate accumulation by ~ 17%. Figure 4 shows the nighttime production of nitrate at different values of γN_2O_5 normalized to the maximum γN_2O_5 value of 0.1. From the sensitivity check, the impact of differences in γN_2O_5 on total nighttime nitrate produced at elevated values of γN_2O_5 (0.1, 0.08, 0.06, 0.04, 0.02, 0.015) is negligible. This is because the model is limited by the availability of N_2O_5 precursor gases such as NO_x and O_3, leading to nighttime N_2O_5 depletion under high γN_2O_5 conditions. When γN_2O_5 is < 0.01, the production of nitrate becomes limited by values of γN_2O_5, rather than oxidant limited. Under low γN_2O_5 (e.g., when γN_2O_5 = 0.001), N_2O_5 does not become depleted, allowing consistent N_2O_5 production throughout the evening and γN_2O_5 to control nitrate production. We note that during this study, the observed 24-hour median value of γN_2O_5 was generally greater than 0.01 for our stable periods, and we did not observe a persistent inversion longer than 3 days. Based on our model results, if a severe inversion event occurred, such as the one observed by Baasandorj et al., (2017), the influence of γN_2O_5 on $PM_{2.5}$ accumulation may be important due to the nitrate effect, which suppresses γN_2O_5 to values lower than 0.01.

https://doi.org/10.5194/egusphere-2026-5384
Preprint. Discussion started: 9 September 2026

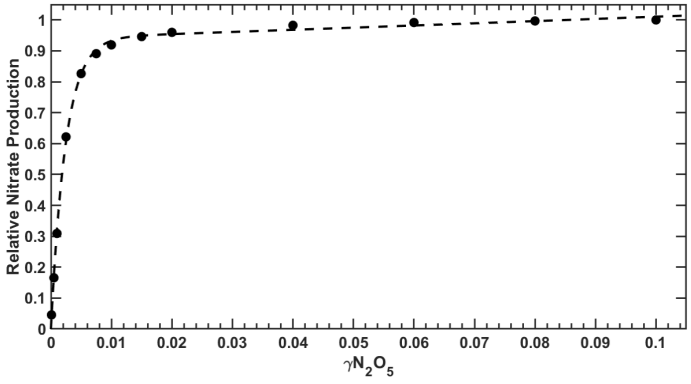

Figure 4: Relative nighttime production of NO_3^- within the residual layer from the 1-D model assuming constant values of γN_2O_5 and no daytime production of NO_3^-. Values of γN_2O_5 for these results are 0.1, 0.08, 0.06, 0.04, 0.02, 0.015, 0.01, 0.0075, 0.005, 0.0025 0.001, 0.0005, 0.0001 (circle markers) and represent values of γN_2O_5 from this study and (McDuffie et al., 2019). The relative nitrate production is calculated as the ratio of end of night (hour 32) nitrate concentration for individual γN_2O_5 values, relative to the end of night nitrate concentration when $\gamma N_2O_5 = 0.1$. The dashed line represents the logarithmic fit of NO_3^- production relative to γN_2O_5.

The 1-D model run and sensitivity check suggests that both oxidant availability and γN_2O_5 play important roles in limiting nighttime nitrate production in SLC. Under high γN_2O_5 conditions, such as those observed at the beginning of inversion periods, the total nighttime production of nitrate is likely oxidant limited. During persistent inversion periods when values of γN_2O_5 decline (< 0.01), the total nighttime production is limited by the nitrate effect. Ambient observations in SLC show that O_3 is typically limited after ~6-days of persistent inversions conditions in SLC (Baasandorj et al., 2017), while we observed a reduction in nitrate aerosol production after 3-4 days due to the aerosol-nitrate effect, highlighting the need for future modeling studies to include both the impact of aerosol chemical composition and oxidant availability when simulating $PM_{2.5}$ accumulation in SLC.

Section 4: Conclusions and Atmospheric Implications

We present the first ambient measurements of γN_2O_5 in SLC to better understand the role of aerosol chemical composition on the rate of nitrate accumulation responsible for wintertime $PM_{2.5}$ pollution events. The results of this study suggest that under clean conditions, values of γN_2O_5 range from 0.018 to 0.16, likely due to the presence of road salts, mineral dust and $(NH_4)_2SO_4$ (Franchin et al., 2018; Hrdina et al., 2021; Moravek et al., 2019) that react efficiently with N_2O_5 (Christie et al., 2025; Gaston & Thornton, 2016; Hu & Abbatt, 1997; Kane et al., 2001; Mitroo et al., 2019; Mozurkewich & Calvert, 1988; Tang et al., 2012, 2014). Under inversion conditions, the accumulation of nitrate inhibits γN_2O_5 due to the well-known nitrate effect (Bertram & Thornton, 2009; Mentel et al., 1999, Wagner et al., 2013). Nitrate is present either through the accumulation of AN on existing aerosol which decreased γN_2O_5 by ~ 0.02 per

https://doi.org/10.5194/egusphere-2026-5384
Preprint. Discussion started: 9 September 2026

day, or through atmospheric aging processes on mineral dust and road salt aerosol (Hrdina et al., 2021; McNamara et al., 2020). The cumulative effects of calcium and sulfate enhancing γN_2O_5 during clean periods, and nitrate inhibiting γN_2O_5 during polluted periods suggests that γN_2O_5 will continually decrease under wintertime inversion conditions as nitrate accumulates in a self-limiting mechanism similar to observations in Colorado by Wagner et al., (2013), likely contributing to the plateaued $PM_{2.5}$ concentrations of 60 to 80 $\mu g/m^3$ observed during persistent inversions.

We support our hypothesis that aerosol nitrate accumulation during inversion events is limited by γN_2O_5 using a 1-D chemical box model. Simulated γN_2O_5 decreases from 0.03 to ~ 0.001 under persistent inversion conditions due to the accumulation of nitrate, while total nighttime nitrate accumulation decreases from 9 $\mu g/m^3$ on the first night to 1 $\mu g/m^3$ on the final night of the simulated inversion event, with maximum nitrate cumulative mass concentrations of ~ 25 $\mu g/m^3$ after the third night of the simulation that remains steady throughout the remaining 2 nights of the simulation. We attribute the consistent mass concentration of nitrate after the third night to the increasing [Sa] within the simulation, which likely offsets depositional losses of aerosol nitrate by promoting reactions with aerosol despite low values of γN_2O_5. Since the model relies on the BT09 parameterization to predict values of γN_2O_5, we are unable to simulate values of γN_2O_5 for mineral dust aerosol periods present during clean periods. By performing 1-day simulations with high values of γN_2O_5, we find that when γN_2O_5 exceeds 0.01, nitrate production becomes limited by the availability of N_2O_5 (representing an oxidant limitation). However, when γN_2O_5 is less than 0.01, the nitrate effect limits nitrate production. Since the model is highly idealized and does not include all potential $nitrate^-$ production mechanisms, the results presented from this model are instead a qualitative perspective on the sensitivity of nitrate production from γN_2O_5. However, our findings suggest that future quantifications of AN accumulation in the SLV should include the effects of particle chemical composition on γN_2O_5. Since aerosol sources are spatially heterogeneous within the SLV (Steenburgh et al., 2012; Lin et al., 2023; Nicoll et al., 2020), additional 3-D modeling analyses that include vertically resolved chemical reactions are likely required. Our model does, however, provide insight into potential constraints on $PM_{2.5}$ accumulation, which can be used to improve assessments of potential control strategies in the future. Our results suggest that gas-phase and particle phase limitations likely contribute to the observed maximum $PM_{2.5}$ mass concentration of 60 – 80 $\mu g/m^3$ observed during persistent inversion events (Baasandorj et al., 2017), highlighting the need to include both particulate phase chemistry and oxidant limitation when predicting wintertime $PM_{2.5}$ pollution in SLC.

Author Contributions:

JAC constructed the AFT, and JAC, LF, and VS tested the AFT and performed in situ data and sample collection with guidance from KAP and CJG. TS, SR, and HPL performed ex-situ soluble ion analysis with guidance from KAP and JAC. AGH and MAG provided laboratory space, logistical support, and guidance for the SLV field study. HH, MAG, and JCL provided the NO_x datasets and assisted with quality assurance. PZ and JAC analyzed the atmospheric

https://doi.org/10.5194/egusphere-2026-5384
Preprint. Discussion started: 9 September 2026

soundings, and PZ aided in their interpretation. SW and JAC built the 1-D chemical model. JAC performed data analysis and wrote the manuscript with input from CJG, KAP, and SW. CJG and KAP designed the field campaign.

Code/Data Availability:

Observations of daily-averaged γN_2O_5 and soluble ion concentrations are tabulated in the supporting information section. Observations of NO_x are unpublished data from the University of Utah Land-Atmosphere Interactions Research Group and can be requested from Prof. John Lin. MesoWest observations of O_3 and $PM_{2.5}$ can be accessed through the website 'mesowest.utah.edu' under the WBB field site (Horel et al., 2002). Potential temperature profiles are publicly available through the Wyoming Weather Lab's atmospheric sounding repository 'weather.uwyo.edu/upperair' site ID 72572. Access to the 1-D chemical model used in this study can be found at 'sites.google.com/view/wangsiyuan/home'.

Competing Interests:

Some authors are members of the editorial board of the journal Atmospheric Chemistry and Physics.

Acknowledgements:

We would like to thank Professor John Horrel (University of Utah) and the MESOWEST team for use of the data from their WBB field site and the University of Utah's Atmospheric Sciences department for their logistical support with the field study. We are grateful to Professor Tim Bertram (University of Wisconsin-Madison) for his assistance with designing and building the AFT. We would also like to thank Professor Joel Thornton (University of Washington Seattle) for the use of his CIMS during the laboratory testing of the AFT.

Financial Support:

This research was supported by the National Oceanic and Atmospheric Administration (NOAA) Atmospheric Chemistry, Carbon Cycle, and Climate Program Awards #NA20OAR4310298 and #NA20OAR4310299.

References:

Ahern, A. T., Goldberger, L., Jahl, L., Thornton, J., & Sullivan, R. C. (2018). Production of N2O5 and ClNO2 through Nocturnal Processing of Biomass-Burning Aerosol. *Environmental Science and Technology*, *52*(2), 550–559. https://doi.org/10.1021/acs.est.7b04386

Baasandorj, M., Hoch, S. W., Bares, R., Lin, J. C., Brown, S. S., Millet, D. B., et al. (2017). Coupling between Chemical and Meteorological Processes under Persistent Cold-Air Pool Conditions: Evolution of Wintertime PM2.5 Pollution Events and N2O5 Observations in

https://doi.org/10.5194/egusphere-2026-5384
Preprint. Discussion started: 9 September 2026

Utah's Salt Lake Valley. *Environmental Science and Technology*, *51*(11), 5941–5950. https://doi.org/10.1021/acs.est.6b06603

Baasandorj, M., Brown, S., Hoch, S., Crosman, E., Long, R., Silva, P., et al. (2018). *2017 Utah Winter Fine Particulate Study Final Report*. Utah.

Behnke, W., George, C., Scheer, V., & Zetzsch, C. (1997). Production and decay of ClNO2 from the reaction of gaseous N2O5 with NaCl solution: Bulk and aerosol experiments. *Journal of Geophysical Research Atmospheres*, *102*(3), 3795–3804. https://doi.org/10.1029/96jd03057

Bertram, T. H., & Thornton, J. A. (2009). Toward a general parameterization of N2O5 reactivity on aqueous particles: the competing effects of particle liquid water, nitrate and chloride. *Atmospheric Chemistry and Physics*, *9*, 8351–8363. Retrieved from www.atmos-chem-phys.net/9/8351/2009/

Bertram, T. H., Thornton, J. A., & Riedel, T. P. (2009). An experimental technique for the direct measurement of N2O5; reactivity on ambient particles. *Atmospheric Measurement Techniques*, *2*(1), 231–242. https://doi.org/10.5194/amt-2-231-2009

Chang, W. L., Bhave, P. V., Brown, S. S., Riemer, N., Stutz, J., & Dabdub, D. (2011). Heterogeneous atmospheric chemistry, ambient measurements, and model calculations of N2O5: A review. *Aerosol Science and Technology*, *45*(6), 665–695. https://doi.org/10.1080/02786826.2010.551672

Christie, J. A., Elliott, H. E., O'Connell-Lopez, S. M. O., Perry, K., Pratt, K. A., Hallar, A. G., et al. (2025). Halogen Production from Playa Dust Emitted from the Great Salt Lake: Implications of the Shrinking Great Salt Lake on Regional Air Quality. *ACS Earth and Space Chemistry*, *9*(3), 480–493. https://doi.org/10.1021/acsearthspacechem.4c00258

Christie, J. A., Pratt, K. A., & Gaston, C. J. (2026). Road-Salt Aerosol Reacts More Efficiently with N2O5 than Sea Spray Aerosol to Produce ClNO2. *ACS Earth and Space Chemistry*, *10*(5), 1418–1428. https://doi.org/10.1021/acsearthspacechem.6c00042

Dentener, F. J., & Crutzen, P. J. (1993). Reaction of N2O5 on tropospheric aerosols: impact on the global distributions of NOx, O3, and OH. *Journal of Geophysical Research*, *98*(D4), 7149–7163. https://doi.org/10.1029/92JD02979

Fountoukis, C., & Nenes, A. (2007). Atmospheric Chemistry and Physics ISORROPIA II: a computationally efficient thermodynamic equilibrium model for K +-Ca 2+-Mg 2+-NH + 4-Na +-SO 2− 4-NO − 3-Cl −-H 2 O aerosols. *Atmos. Chem. Phys*, *7*, 4639–4659. Retrieved from www.atmos-chem-phys.net/7/4639/2007/

Franchin, A., Fibiger, D. L., Goldberger, L., McDuffie, E. E., Moravek, A., Womack, C. C., et al. (2018). Airborne and ground-based observations of ammonium-nitrate-dominated aerosols in a shallow boundary layer during intense winter pollution episodes in northern Utah.

https://doi.org/10.5194/egusphere-2026-5384
Preprint. Discussion started: 9 September 2026

Atmospheric Chemistry and Physics, *18*(23), 17259–17276. https://doi.org/10.5194/acp-18-17259-2018

Fuchs, N. A., & Sutugin, A. G. (1971). High Dispersed Aerosols. In *Topics in Current Aerosol Research* (p. 1). Elsevier. https://doi.org/10.1016/B978-0-08-016674-2.50006-6

Gaston, C. J., & Thornton, J. A. (2016). Reacto-Diffusive Length of N2O5 in Aqueous Sulfate- and Chloride-Containing Aerosol Particles. *Journal of Physical Chemistry A*, *120*(7), 1039–1045. https://doi.org/10.1021/acs.jpca.5b11914

Gaston, C. J., Riedel, T. P., Zhang, Z., Gold, A., Surratt, J. D., & Thornton, J. A. (2014). Reactive uptake of an isoprene-derived epoxydiol to submicron aerosol particles. *Environmental Science and Technology*, *48*(19), 11178–11186. https://doi.org/10.1021/es5034266

Gaston, C. J., Thornton, J. A., & Ng, N. L. (2014). Reactive uptake of N2O5 to internally mixed inorganic and organic particles: The role of organic carbon oxidation state and inferred organic phase separations. *Atmospheric Chemistry and Physics*, *14*(11), 5693–5707. https://doi.org/10.5194/acp-14-5693-2014

Gaston, C. J., Pratt, K. A., Suski, K. J., May, N. W., Gill, T. E., & Prather, K. A. (2017). Laboratory Studies of the Cloud Droplet Activation Properties and Corresponding Chemistry of Saline Playa Dust. *Environmental Science & Technology*, *51*(3), 1348–1356. https://doi.org/10.1021/acs.est.6b04487

Gaston, Cassandra J. (2020). Re-examining Dust Chemical Aging and Its Impacts on Earth's Climate. *Accounts of Chemical Research*, *53*(5), 1005–1013. https://doi.org/10.1021/acs.accounts.0c00102

Hansen, J. C., Woolwine III, W. R., Bates, B. L., Clark, J. M., Kuprov, R. Y., Mukherjee, P., et al. (2010). Semicontinuous PM2.5 and PM10 Mass and Composition Measurements in Lindon, Utah, during Winter 2007. *Journal of the Air & Waste Management Association*, *60*(3), 346–355. https://doi.org/10.3155/1047-3289.60.3.346

Horel, J., Splitt, M., Dunn, L., Pechmann, J., White, B., Ciliberti, C., et al. (2002). Mesowest: Cooperative Mesonets in the Western United States. *Bulletin of the American Meteorological Society*, *83*(2), 211–225. https://doi.org/10.1175/1520-0477(2002)083<0211:MCMITW>2.3.CO;2

Hrdina, A., Murphy, J. G., Hallar, A. G., Lin, J. C., Moravek, A., Bares, R., et al. (2021). The role of coarse aerosol particles as a sink of HNO3 in wintertime pollution events in the Salt Lake Valley. *Atmospheric Chemistry and Physics*, *21*(10), 8111–8126. https://doi.org/10.5194/acp-21-8111-2021

https://doi.org/10.5194/egusphere-2026-5384
Preprint. Discussion started: 9 September 2026

687 Hu, J. H., & Abbatt, J. P. D. (1997). Reaction Probabilities for N2O5 Hydrolysis on Sulfuric Acid
688 and Ammonium Sulfate Aerosols at Room Temperature. *The Journal of Physical Chemistry*
689 *A*, *101*(5), 871–878. https://doi.org/10.1021/jp9627436

690 Isaacman-VanWertz, G., Sueper, D. T., Aikin, K. C., Lerner, B. M., Gilman, J. B., de Gouw, J. A.,
691 et al. (2017). Automated single-ion peak fitting as an efficient approach for analyzing
692 complex chromatographic data. *Journal of Chromatography A*, *1529*, 81–92.
693 https://doi.org/10.1016/j.chroma.2017.11.005

694 Ivey, C. E., Balachandran, S., Colgan, S., Hu, Y., & Holmes, H. A. (2019). Investigating fine
695 particulate matter sources in Salt Lake City during persistent cold air pool events.
696 *Atmospheric Environment*, *213*, 568–578. https://doi.org/10.1016/j.atmosenv.2019.06.042

697 James Steenburgh, W., Massey, J. D., & Painter, T. H. (2012). Episodic dust events of Utah's
698 wasatch front and adjoining region. *Journal of Applied Meteorology and Climatology*,
699 *51*(9), 1654–1669. https://doi.org/10.1175/JAMC-D-12-07.1

700 Jenkin, M. E., Saunders, S. M., Wagner, V., & Pilling, M. J. (2003). Protocol for the development
701 of the Master Chemical Mechanism, MCM v3 (Part B): tropospheric degradation of
702 aromatic volatile organic compounds. *Atmospheric Chemistry and Physics*, *3*(1), 181–193.
703 https://doi.org/10.5194/acp-3-181-2003

704 Jeong, D., McNamara, S. M., Chen, Q., Mirrielees, J., Edebeli, J., Kulju, K. D., et al. (2023).
705 Quantifying the Contributions of Aerosol- and Snow-Produced ClNO2 through
706 Observations and 1D Modeling. *ACS Earth and Space Chemistry*, *7*(12), 2548–2561.
707 https://doi.org/10.1021/acsearthspacechem.3c00237

708 Kane, S. M., Caloz, F., & Leu, M.-T. (2001). Heterogeneous Uptake of Gaseous N2O5 by
709 (NH4)2SO4, NH4HSO4, and H2SO4 Aerosols. *The Journal of Physical Chemistry A*,
710 *105*(26), 6465–6470. https://doi.org/10.1021/jp010490x

711 Kelly, K. E., Kotchenruther, R., Kuprov, R., & Silcox, G. D. (2013). Receptor model source
712 attributions for Utah's Salt Lake City airshed and the impacts of wintertime secondary
713 ammonium nitrate and ammonium chloride aerosol. *Journal of the Air & Waste*
714 *Management Association*, *63*(5), 575–590. https://doi.org/10.1080/10962247.2013.774819

715 Kolesar, K. R., Mattson, C. N., Peterson, P. K., May, N. W., Prendergast, R. K., & Pratt, K. A.
716 (2018). Increases in wintertime PM2.5 sodium and chloride linked to snowfall and road salt
717 application. *Atmospheric Environment*, *177*, 195–202.
718 https://doi.org/10.1016/j.atmosenv.2018.01.008

719 Kuprov, R., Eatough, D. J., Cruickshank, T., Olson, N., Cropper, P. M., & Hansen, J. C. (2014).
720 Composition and secondary formation of fine particulate matter in the Salt Lake Valley:
721 Winter 2009. *Journal of the Air & Waste Management Association*, *64*(8), 957–969.
722 https://doi.org/10.1080/10962247.2014.903878

https://doi.org/10.5194/egusphere-2026-5384
Preprint. Discussion started: 9 September 2026

Lareau, N. P., Crosman, E., Whiteman, C. D., Horel, J. D., Hoch, S. W., Brown, W. O. J., & Horst, T. W. (2013). The persistent cold-air pool study. *Bulletin of the American Meteorological Society*, *94*(1), 51–63. https://doi.org/10.1175/BAMS-D-11-00255.1

Li, J., Zhai, T., Chen, X., Wang, H., Xie, S., Chen, S., et al. (2025). Direct measurement of N2O5 heterogeneous uptake coefficients on atmospheric aerosols in southwestern China and evaluation of current parameterizations. *Atmospheric Chemistry and Physics*, *25*(12), 6395–6406. https://doi.org/10.5194/acp-25-6395-2025

Liao, J., Sihler, H., Huey, L. G., Neuman, J. A., Tanner, D. J., Friess, U., et al. (2011). A comparison of Arctic BrO measurements by chemical ionization mass spectrometry and long path-differential optical absorption spectroscopy. *Journal of Geophysical Research*, *116*, D00R02. https://doi.org/10.1029/2010JD014788

Lin, J. C., Fasoli, B., Mitchell, L., Bares, R., Hopkins, F., Thompson, T. M., & Alvarez, R. A. (2023). Towards hyperlocal source identification of pollutants in cities by combining mobile measurements with atmospheric modeling. *Atmospheric Environment*, *311*, 119995. https://doi.org/10.1016/j.atmosenv.2023.119995

Lyu, C., Harkins, C., Li, M., Mueller, K., Prothero, J., Verreyken, B., et al. (2025). Development of the United States GReenhouse Gas and Air Pollutants Emissions System (GRA2PES). *Journal of Geophysical Research: Atmospheres*, *130*(20). https://doi.org/10.1029/2025JD043597

Mangelson, N. F., Lewis, L., Joseph, J. M., Cui, W., Machir, J., Eatough, D. J., et al. (1997). The Contribution of Sulfate and Nitrate to Atmospheric Fine Particles During Winter Inversion Fogs in Cache Valley, Utah. *Journal of the Air & Waste Management Association*, *47*(2), 167–175. https://doi.org/10.1080/10473289.1997.10464429

McDuffie, E. E., Womack, C. C., Fibiger, D. L., Dube, W. P., Franchin, A., Middlebrook, A. M., et al. (2019). On the contribution of nocturnal heterogeneous reactive nitrogen chemistry to particulate matter formation during wintertime pollution events in Northern Utah. *Atmospheric Chemistry and Physics*, *19*(14), 9287–9308. https://doi.org/10.5194/acp-19-9287-2019

McNamara, S. M., Raso, A. R. W., Wang, S., Thanekar, S., Boone, E. J., Kolesar, K. R., et al. (2019). Springtime Nitrogen Oxide-Influenced Chlorine Chemistry in the Coastal Arctic. *Environmental Science & Technology*, *53*(14), 8057–8067. https://doi.org/10.1021/acs.est.9b01797

McNamara, S. M., Kolesar, K. R., Wang, S., Kirpes, R. M., May, N. W., Gunsch, M. J., et al. (2020). Observation of Road Salt Aerosol Driving Inland Wintertime Atmospheric Chlorine Chemistry. *ACS Central Science*, *6*(5), 684–694. https://doi.org/10.1021/acscentsci.9b00994

https://doi.org/10.5194/egusphere-2026-5384
Preprint. Discussion started: 9 September 2026

Mentel, T. F., Sohn, M., & Wahner, A. (1999). Nitrate effect in the heterogeneous hydrolysis of dinitrogen pentoxide on aqueous aerosols. *Physical Chemistry Chemical Physics*, *1*(24), 5451–5457. https://doi.org/10.1039/a905338g

Mitroo, D., Gill, T. E., Haas, S., Pratt, K. A., & Gaston, C. J. (2019). ClNO2 Production from N2O5 Uptake on Saline Playa Dusts: New Insights into Potential Inland Sources of ClNO2. *Environmental Science & Technology*, *53*(13), 7442–7452. https://doi.org/10.1021/acs.est.9b01112

Moravek, A., Murphy, J. G., Hrdina, A., Lin, J. C., Pennell, C., Franchin, A., et al. (2019). Wintertime spatial distribution of ammonia and its emission sources in the Great Salt Lake region. *Atmospheric Chemistry and Physics*, *19*(24), 15691–15709. https://doi.org/10.5194/acp-19-15691-2019

Morris, E. D., & Niki, H. (1973). Reaction of dinitrogen pentoxide with water. *The Journal of Physical Chemistry*, *77*(16), 1929–1932. https://doi.org/10.1021/j100635a001

Mozurkewich, M., & Calvert, J. G. (1988). Reaction probability of N2O5 on aqueous aerosols. *Journal of Geophysical Research*, *93*(D12). https://doi.org/10.1029/jd093id12p15889

Nicoll, K., Hahnenberger, M., & Goldstein, H. L. (2020). 'Dust in the wind' from source-to-sink: Analysis of the 14–15 April 2015 storm in Utah. *Aeolian Research*, *46*. https://doi.org/10.1016/j.aeolia.2019.06.002

Petersen, R. C., Hallar, A. G., McCubbin, I. B., Ogren, J. A., Andrews, E., Lowenthal, D., et al. (2019). Numerical, wind-tunnel, and atmospheric evaluation of a turbulent ground-based inlet sampling system. *Aerosol Science and Technology*, *53*(6), 712–727. https://doi.org/10.1080/02786826.2019.1602718

Riedel, T. P., Bertram, T. H., Ryder, O. S., Liu, S., Day, D. A., Russell, L. M., et al. (2012). Direct N2O5 reactivity measurements at a polluted coastal site. *Atmospheric Chemistry and Physics*, *12*(6), 2959–2968. https://doi.org/10.5194/acp-12-2959-2012

Roberts, J. M., Osthoff, H. D., Brown, S. S., Ravishankara, A. R., Coffman, D., Quinn, P., & Bates, T. (2009). Laboratory studies of products of N2O5 uptake on Cl- containing substrates. *Geophysical Research Letters*, *36*(20). https://doi.org/10.1029/2009GL040448

Royer, H. M., Mitroo, D., Hayes, S. M., Haas, S. M., Pratt, K. A., Blackwelder, P. L., et al. (2021). The role of hydrates, competing chemical constituents, and surface composition on ClNO2 Formation. *Environmental Science and Technology*, *55*(5), 2869–2877. https://doi.org/10.1021/acs.est.0c06067

Saunders, S. M., Jenkin, M. E., Derwent, R. G., & Pilling, M. J. (2003). Protocol for the development of the Master Chemical Mechanism, MCM v3 (Part A): tropospheric

https://doi.org/10.5194/egusphere-2026-5384
Preprint. Discussion started: 9 September 2026

degradation of non-aromatic volatile organic compounds. *Atmospheric Chemistry and Physics*, *3*(1), 161–180. https://doi.org/10.5194/acp-3-161-2003

Schnell, R. C., Oltmans, S. J., Neely, R. R., Endres, M. S., Molenar, J. V., & White, A. B. (2009). Rapid photochemical production of ozone at high concentrations in a rural site during winter. *Nature Geoscience*, *2*(2), 120–122. https://doi.org/10.1038/ngeo415

Shiraiwa, M., Zuend, A., Bertram, A. K., & Seinfeld, J. H. (2013). Gas–particle partitioning of atmospheric aerosols: interplay of physical state, non-ideal mixing and morphology. *Physical Chemistry Chemical Physics*, *15*(27), 11441. https://doi.org/10.1039/c3cp51595h

Silcox, G. D., Kelly, K. E., Crosman, E. T., Whiteman, C. D., & Allen, B. L. (2011). Wintertime PM2.5 concentrations during persistent, multi-day cold-air pools in a mountain valley. *Atmospheric Environment*. https://doi.org/10.1016/j.atmosenv.2011.10.041

Staudt, S., Gord, J. R., Karimova, N. V., McDuffie, E. E., Brown, S. S., Gerber, R. B., et al. (2019). Sulfate and Carboxylate Suppress the Formation of ClNO2 at Atmospheric Interfaces. *ACS Earth and Space Chemistry*, *3*(9), 1987–1997. https://doi.org/10.1021/acsearthspacechem.9b00177

Stewart, D. J., Griffiths, P. T., & Cox, R. A. (2004). *Atmospheric Chemistry and Physics Reactive uptake coefficients for heterogeneous reaction of N 2 O 5 with submicron aerosols of NaCl and natural sea salt*. *Atmos. Chem. Phys* (Vol. 4). Retrieved from www.atmos-chem-phys.org/acp/4/1381/

Sun, X., & Holmes, H. A. (2019). Surface turbulent fluxes during persistent cold-air pool events in the salt lake valley, Utah. Part I: Observations. *Journal of Applied Meteorology and Climatology*, *58*(12), 2553–2568. https://doi.org/10.1175/JAMC-D-19-0053.1

Tang, M. J., Thieser, J., Schuster, G., & Crowley, J. N. (2012). Kinetics and mechanism of the heterogeneous reaction of N 2O 5 with mineral dust particles. *Physical Chemistry Chemical Physics*, *14*(24), 8551–8561. https://doi.org/10.1039/c2cp40805h

Tang, M. J., Schuster, G., & Crowley, J. N. (2014). Heterogeneous reaction of N2O5 with illite and Arizona test dust particles. *Atmospheric Chemistry and Physics*, *14*(1), 245–254. https://doi.org/10.5194/acp-14-245-2014

Thornton, J. A., & Abbatt, J. P. D. (2005). N2O5 reaction on submicron sea salt aerosol: Kinetics, products, and the effect of surface active organics. *Journal of Physical Chemistry A*, *109*(44), 10004–10012. https://doi.org/10.1021/jp054183t

Wagner, N. L., Riedel, T. P., Young, C. J., Bahreini, R., Brock, C. A., Dubé, W. P., et al. (2013). N2O5 uptake coefficients and nocturnal NO2 removal rates determined from ambient wintertime measurements. *Journal of Geophysical Research Atmospheres*, *118*(16), 9331–9350. https://doi.org/10.1002/jgrd.50653

https://doi.org/10.5194/egusphere-2026-5384
Preprint. Discussion started: 9 September 2026

827 Wang, S., & Pratt, K. A. (2017). Molecular Halogens Above the Arctic Snowpack: Emissions,
828 Diurnal Variations, and Recycling Mechanisms. *Journal of Geophysical Research:*
829 *Atmospheres*, *122*(21). https://doi.org/10.1002/2017JD027175

830 Wang, S., McNamara, S. M., Kolesar, K. R., May, N. W., Fuentes, J. D., Cook, R. D., et al.
831 (2020). Urban Snowpack ClNO2 Production and Fate: A One-Dimensional Modeling Study.
832 *ACS Earth and Space Chemistry*, *4*(7), 1140–1148.
833 https://doi.org/10.1021/acsearthspacechem.0c00116

834 Wexler, A. S., & Clegg, S. L. (2002). Atmospheric aerosol models for systems including the ions
835 H+ , NH4+ , Na+ , SO42- , NO3-, Cl-, Br-, and H2O. *Journal of Geophysical Research:*
836 *Atmospheres*, *107*(D14). https://doi.org/10.1029/2001JD000451

837 Whiteman, C. D., Hoch, S. W., Horel, J. D., & Charland, A. (2014). Relationship between
838 particulate air pollution and meteorological variables in Utah's Salt Lake Valley.
839 *Atmospheric Environment*, *94*, 742–753. https://doi.org/10.1016/j.atmosenv.2014.06.012

840

841